ELSEVIER

Journal of Alloys and Compounds 253–254 (1997) 564–569

Journal of ALLOYS AND COMPOUNDS

Electrochemical performances of ZrM_2 (M=V, Cr, Mn, Ni) Laves phases and the relation to microstructures and thermodynamical properties

J.-M. Joubert, Dalin Sun, M. Latroche, A. Percheron-Guégan*

Laboratoire de Chimie Métallurgique et Spectroscopie des Terres Rares C.N.R.S., 1, Place Aristide Briand, 92195 Meudon Cedex, France

Received 26 August 1996; revised 8 November 1996

Abstract

Zr-based AB_2 (B=V, Cr, Mn) Laves phases are studied for their ability to reversibly store hydrogen and are potential negative electrode materials in Ni–MH batteries. The hydrides formed are too stable for electrochemical use and their thermodynamical properties can be adapted by Ni substitution on the B sublattice. However, measured electrochemical reversible capacities are very low compared to solid–gas results. This phenomenon is related to passivation and surface corrosion in electrolytic medium. To overcome this problem, the role of secondary phases has been studied following two routes: precipitation of controlled amounts of Zr–Ni binary intermetallic compounds or addition of a rare earth (R) element leading to precipitation of RNi compound in the matrix. The consequences on the electrochemical behaviour are discussed in terms of the microstructure of the alloys which lead to composite electrodes by taking advantage of the bulk properties of the Laves phase and the surface properties of the secondary phase(s).

Keywords: Zr-based Laves phases; Hydrides; Nickel-hydride batteries; Secondary phases; Activation

1. Introduction

The use of Zr-based AB_2 alloys as electrodes in nickel–metal hydride batteries has been intensively studied in recent years. This is due to their large hydrogen reversible capacity compared with AB_5-type compounds presently used in commercial devices. However, unlike these last compounds, their electrochemical capacities are often lower than that determined from solid–gas reaction. This phenomenon is related to an interface reaction with the electrolyte. Passivation or surface corrosion induce difficult activation, low kinetics and even blocking of the electrochemical reaction. In order to overcome these problems, the role of precipitated secondary phases within the Laves phase has been studied following two routes:

(i) The synthesis of alloys for which a Zr–Ni binary intermetallic compound such as Zr_7Ni_{10} is in equilibrium with the Laves phase $Zr(Cr_{1-x}Ni_x)_2$ in controlled amounts [1,2].

(ii) The addition of small amounts of rare earth (R) to the same Laves phase, which seems to efficiently improve hydriding behaviour [3–6].

The hydriding characteristics in solid–gas and electrochemical reactions of the pure Laves phase $Zr(Cr_{0.4}Ni_{0.6})_2$, which is considered a model compound is compared with samples containing different amounts and types of secondary phases. The beneficial role played by these phases is checked in a multicomponent compound $Zr(Ni_{0.6}Mn_{0.3}V_{0.1}Cr_{0.05})_2$ which exhibits a very important electrochemical capacity [7,8]. The improved hydriding behaviour is related to the microstructure of the alloys. The H absorption mechanism at the interface between the electrolyte and the alloy surface is described and a schematic model is proposed.

2. Experimental procedures

The experimental procedures have been described in detail [1,2,6,8]. The intermetallic compounds were synthesized by induction melting of the pure elements generally followed by appropriate annealing. They were characterized by metallographic observation, electron probe microanalysis (EPMA) and X-ray diffraction (XRD) experiments. The hydrogenation experiments were carried out by using the conventional volumetric method. The electro-

*Corresponding author.

0925-8388/97/$17.00
PII S0925-8388(96)03088-5

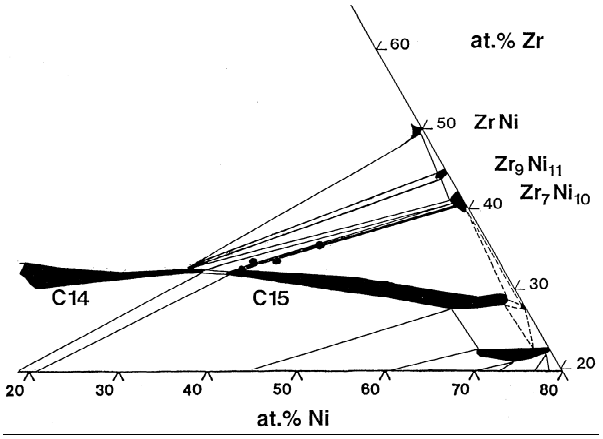

Fig. 1. Partial phase diagram of the Zr–Ni–Cr system showing the equilibria between the Laves phases and the binary Zr–Ni compounds.

chemical measurements were done by galvanostatic charging and discharging nickel–metal hydride batteries.

3. Ternary Zr–Ni–Cr system

3.1. Synthesis of two-phase alloys

The determination of the Zr–Ni–Cr phase diagram at 1000 °C permits description of the alloys located around the stoichiometric AB_2 line: $Zr(Cr_{1-x}Ni_x)_2$ [1,2]. The cubic C15 structure of $ZrCr_2$ is retained for low nickel substitutions. At higher nickel contents it is transformed into the hexagonal C14 structure up to the composition $Zr(Cr_{0.5}Ni_{0.5})_2$. From the composition $Zr(Cr_{0.4}Ni_{0.6})_2$ onwards a change is observed and the C15 structure extends up to $Zr(Cr_{0.05}Ni_{0.95})_2$. Each single phase domain is separated by two-phase (C14 plus C15) domains. The replacement of chromium by nickel involves a constant decrease in cell volume as expected from the smaller atomic radius of nickel. The substitution is also accompanied by a progressive decrease of zirconium content in the phase which causes the precipitation of secondary phases when near-stoichiometric AB_2 samples are synthesized.

From these results, different alloys are synthesized with nominal compositions following the tie line in the phase diagram from the single C15 phase $Zr(Cr_{0.4}Ni_{0.6})_2$ to the binary Zr_7Ni_{10} compound (Fig. 1). The characterization of the alloys described in Table 1 shows the progressive increase in the amount of Zr_7Ni_{10} phase in the alloy without a significant change of the cell parameter of the Laves phase.

3.2. Solid–gas and electrochemical properties of single $Zr(Cr_{1-x}Ni_x)_2$ phase

The PCT isotherms of $Zr(Cr_{1-x}Ni_x)_2$ with $x=0.5$; 0.6; 0.7; 0.8 [2] show that the plateau pressure increases linearly with the decrease of the intermetallic cell volume and that the reversible capacity increases up to $Zr(Cr_{0.5}Ni_{0.5})_2$ and then decreases. Fig. 2 allows one to choose the best composition for which the plateau pressure at room temperature (about 0.4 bar) is well adapted for electrochemical application and which exhibits a reversible capacity of 3 H/f.u. (i.e. 400 mAh g^{-1}): $x=0.6$.

The results of electrochemical charge and discharge for this compound are presented in Table 2. The capacities are extremely poor compared to that measured by solid–gas reaction. The charge of the electrode in a sealed cell equipped with a pressure gauge reveals that the low

Table 1
Characterization of Zr–Ni–Cr alloys used for solid–gas and electrochemical measurements

Nominal composition (at.%)			Phases	Weight ratio (%)	Composition (at.%)			Cell parameters (Å)	Cell volume (Å^3/AB_2)
Zr	Ni	Cr			Zr	Ni	Cr		
See [2]			C15	100	31.6	37.8	30.6	$a=7.070$	44.18
33.3	40.0	26.6	C15	91	32.3	39.1	29	$a=7.066$	44.11
			Zr_7Ni_{10}	9	41.3	57.2	1.5	$a=9.220$ $b=9.200$ $c=12.346$	
33.5	42.5	24	C15	85	31.9	40.9	27.1	$a=7.060$	43.99
			Zr_7Ni_{10}	15	40.7	57.9	1.4	$a=9.206$ $b=9.183$ $c=12.347$	
35.5	46.25	18.25	C15	64	32.1	41.3	26.7	$a=7.061$	44.00
			Zr_7Ni_{10}	36	41.0	57.6	1.4	$a=9.204$ $b=9.183$ $c=12.352$	
41.2	58.8	–	Zr_7Ni_{10}	100	41.1	58.9	–	$a=9.199$ $b=9.158$ $c=12.352$	

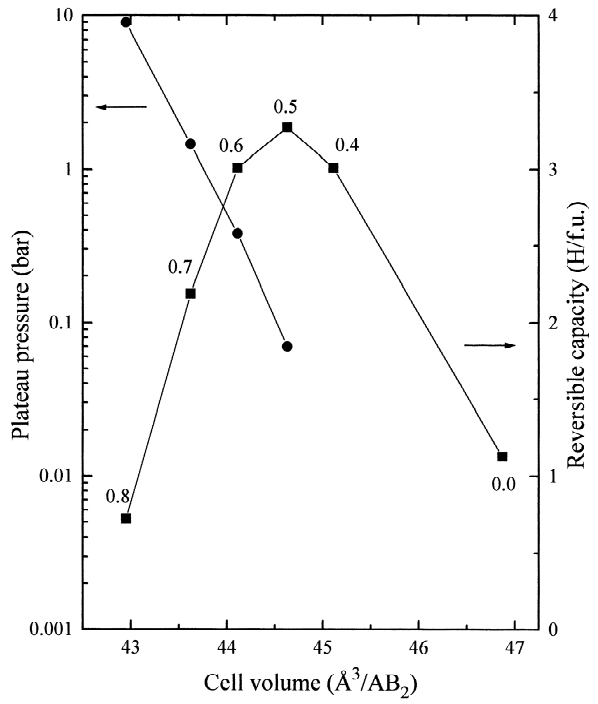

Fig. 2. Variation of the plateau pressure and the reversible capacity of $Zr(Cr_{1-x}Ni_x)_2$ Laves phase as a function of cell volume of the intermetallics (from [2]).

capacity is linked to hydrogen gas evolution which starts from the very beginning of the charge. This is probably due to a surface passivation in electrolytic medium which inhibits the transfer of hydrogen from the electrolyte to the bulk material.

At this stage, the surface treatment with dilute hydrofluoric acid, successfully used by Züttel et al. [9] for $Zr(V_{1-x}Ni_x)_2$ electrodes, was tried. The charge and discharge capacity in the first cycle is 215 mAh g^{-1} but the discharge capacity decreases rapidly with cycling and after ten cycles returns to the value obtained for the non-treated electrode. This result is explained by the absence of electrochemical charge related to surface passivation and demonstrates the necessity of modifying the surface properties of the grains to improve the electrode behaviour. This modification can be obtained by secondary phase precipitation at controlled rates.

Table 2
Electrochemical discharge capacity of the single Laves phase alloy

$Zr(Cr_{0.4}Ni_{0.6})_2$	mAh g^{-1}
Absorption capacity in solid–gas reaction (25 °C, 10 bar)	400
Electrochemical charge capacity (40 mA g^{-1})	35
Electrochemical discharge capacity (80+40+20 mA g^{-1}) (mAh g^{-1})	25
Electrochemical discharge capacity after HF treatment (1%, 5 min)	215 (1st cycle) 25 (after 10 cycles)

Table 3
Electrochemical discharge capacity of the single and two phase alloys

Alloy	Capacity at 20 mA g^{-1} current (mAh g^{-1})
$Zr(Cr_{0.4}Ni_{0.6})_2=AB_2$	25
AB_2+9% Zr_7Ni_{10}	227
AB_2+15% Zr_7Ni_{10}	263
AB_2+36% Zr_7Ni_{10}	227
Zr_7Ni_{10}	50

3.3. Electrochemical capacities of two-phase $Zr(Cr_{0.4}Ni_{0.6})_2$ alloys

The electrochemical capacities of the alloys described in Table 1 are listed in Table 3. In Fig. 3 the total discharge capacities are plotted as a function of secondary phase content and compared with the capacity discharged by the Laves phase. The latter was calculated by assuming that the secondary phase has a constant capacity equal to that measured previously [2]. A spectacular increase of the global discharge capacity is observed. It reaches a maximum at around 20% of secondary phase and then decreases with increasing amount of the low capacity phase. In contrast, the real discharge capacity of the Laves phase tends to reach a limit of 330 mAh g^{-1}.

The Laves phase has a reversible hydrogen capacity measured by solid–gas reaction of 400 mAh g^{-1}, of which 90% is absorbed between 0.1 and 10 bar. This pressure range is compatible with the electrochemical reversibility region. However, discharge capacities are low because hydrogen transfer from the electrolyte into the bulk material is inhibited at the interface by a passivation layer.

On the other hand, the Zr_7Ni_{10} phase has a high hydrogen capacity in solid–gas reaction (370 mAh g^{-1}) but a small capacity when studied in the electrochemically reversible pressure range (40 mAh g^{-1}) due to the great

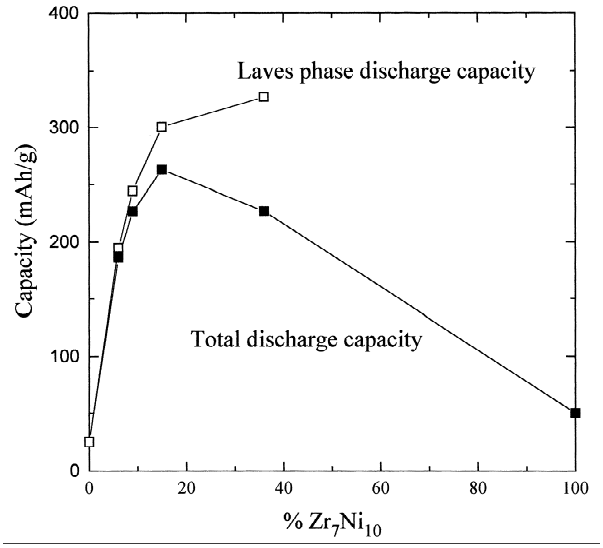

Fig. 3. Discharge capacities (■ total), (□ Laves phase) as a function of secondary phase content in the alloy.

stability and low reversibility of the hydride at room temperature [10]. The electrochemical capacity (50 mAh g^{-1}) is in agreement with this second value. This means a correct electrochemical process and an absence of interfacial problems.

In the grains involved in the electrochemical reaction, two phases are finely mixed with respect to the grain size, one having interesting bulk properties but a blocking surface, and the other having a surface which allows a electrochemical reaction but having inadequate thermodynamic properties. For these reasons the two phases exhibit very low discharge capacity when used separately. The considerable enhancement of the discharge capacity in the two-phase alloy is explained by the modification of the grain surface and by the presence of the precipitated secondary phase on this surface. A beneficial effect of the presence of the secondary phase Zr_7Ni_{10} has also been recently observed in $Zr(V_{0.25}Ni_{0.75})_2$ two-phase alloys [11].

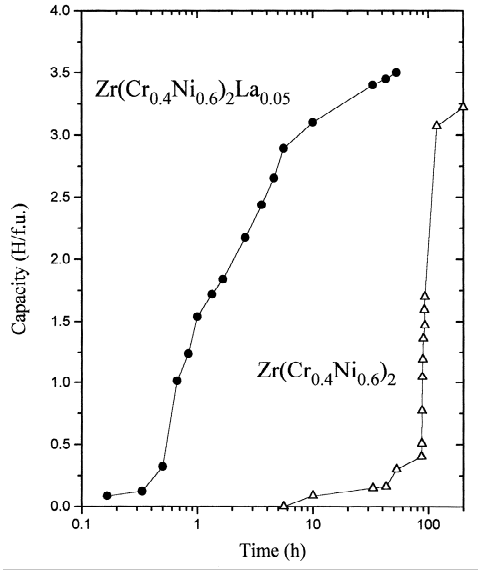

Fig. 4. Effect of La addition in $Zr(Cr_{0.4}Ni_{0.6})_2$ on the initial hydrogen absorbing curves.

4. Addition of rare earth

4.1. Addition to $Zr(Cr_{0.4}Ni_{0.6})_2$

Recently, following the easy activation of $LaNi_5$ type electrodes, Kim and Lee [3] observed that the activation of hexagonal C14 type $Zr(Cr_{0.5}Ni_{0.5})_2$ was greatly improved by adding light rare earth elements. They assumed that this improvement can be attributed to the formation of a second phase Cr_3Ni_2 identified in the XRD patterns of the alloys.

Lanthanum was added to cubic C15 type $Zr(Cr_{0.4}Ni_{0.6})_2$. The metallurgical state of lanthanum was examined and its effects on the activation behaviour were also investigated in solid–H_2 gas reaction as well as in an alkaline electrolyte [6]. The characterizations by XRD and EPMA of the pure and $La_{0.05}$ added $Zr(Cr_{0.4}Ni_{0.6})_2$ samples are presented in Table 4. For both alloys, EPMA shows that the majority phase is the Laves phase $Zr(Cr_{0.4}Ni_{0.6})_2$. For the $La_{0.05}$ added sample, a second phase is precipitated dispersively in the matrix and was identified as the definite compound LaNi. The XRD patterns revealed that the matrix of the two alloys had the cubic C15 structure with the same cell parameters. This means that lanthanum did not dissolve into the Laves phase. The LaNi compound was not detected by XRD due to the very small amount in the alloy which was estimated to be less than 5%.

The comparison of the activation behaviour in solid–H_2 gas reaction is shown in Fig. 4. It indicates that the pure Laves phase begins to absorb after a 6-h incubation period and about 90 h are necessary to reach full absorption. With La addition, the absorption begins after only 40 min and the full capacity (3.5 H/f.u.) is reached after about 10 h.

The dependence of discharge capacities on charging and discharging cycles is shown in Fig. 5. The discharge capacity of the pure Laves phase increases very slowly with the number of cycles but remains below 100 mAh g^{-1} even after 10 cycles. On the other hand the initial discharge capacity of $Zr(Cr_{0.4}Ni_{0.6})_2La_{0.05}$ reaches 230 mAh g^{-1} which is very close to the measured maximum value.

The poor activation of the pure Laves phase can be attributed to a surface oxide layer formed in air or in contact with the electrolyte. The activation can be improved by the presence of the LaNi phase which is finely dispersed in the matrix. LaNi can readily absorb large amounts of hydrogen at room temperature by forming a stable hydride [12] and may be regarded as an ‘active site’ which allows hydrogen atoms to penetrate easily through the oxide layer.

Table 4
Metallurgical state of lanthanum in La added C15 phase

Alloy	Phases	Cell parameter (Å)	Composition (at.%)			
			Zr	Cr	Ni	La
$Zr(Cr_{0.4}Ni_{0.6})_2$	C15	a=7.059(1)	30.5	40.1	29.4	–
$Zr(Cr_{0.4}Ni_{0.6})_2La_{0.05}$	C15	a=7.058(1)	31.5	36.3	32.2	0
	LaNi		2.4	1.7	47.6	48.3

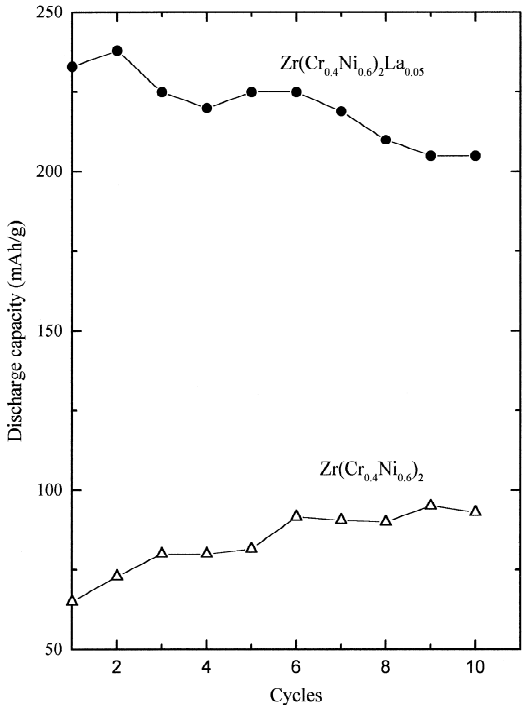

Fig. 5. Dependence of discharge electrochemical capacities on cycling.

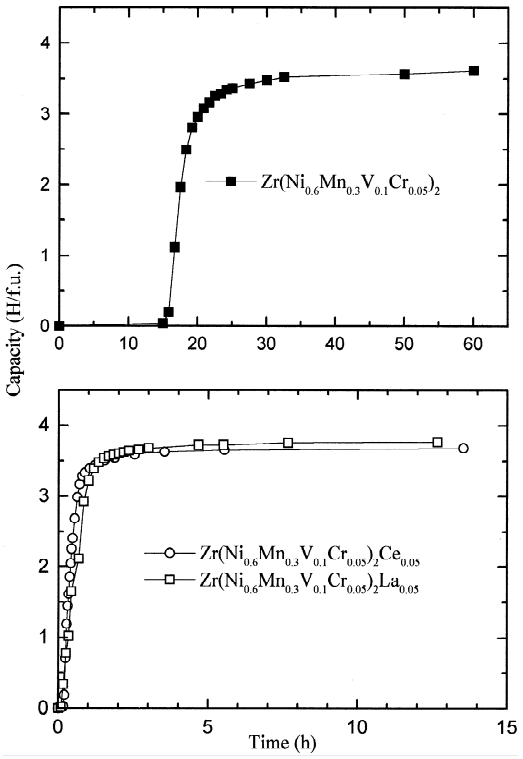

Fig. 6. Effect of La and Ce additions in multicomponent Zr–Ni–Mn–V–Cr Laves phase on the initial hydrogen absorbing curves.

4.2. Addition to multicomponent Zr–Ni–Mn–V–Cr Laves phase

In spite of the improvement of the hydrogen absorbing properties of pseudobinary Laves phases by precipitation of a secondary phase, the values of the electrochemical capacity remain too low for industrial applications. So, the effect of the same light rare earth addition in a multicomponent C15 Laves phase $Zr(Ni_{0.6}Mn_{0.3}V_{0.1}Cr_{0.05})_2$ exhibiting large hydrogen storage capacity [7] has been studied. Two rare earth elements, lanthanum and cerium were added separately to prepare $ZrNi_{1.2}Mn_{0.6}V_{0.2}Cr_{0.1}X_{0.05}$ (X=La or Ce). The characterization of the pure Laves phase and the rare earth added compounds are summarized in Table 5. As in the previous case the EPMA indicates that the matrix is still the Laves phase and that secondary phases corresponding to the compositions LaNi and CeNi are well distributed. The solubility of lanthanum or cerium in the matrix is zero. XRD reveals that the Laves phase of the three alloys has the cubic C15 structure and that the cell parameters are the same within the experimental error. However no peaks from LaNi or CeNi can be seen due to their low concentrations.

The activation behaviour in the solid–H_2 gas reaction of the three alloys is compared in Fig. 6. For the pure Laves phase alloys, the absorption begins after 15 h incubation whereas those with rare earth additions immediately absorb hydrogen up to full capacity (3.6 H/f.u.).

The dependence of discharge capacity on cycle number of the three alloys is shown in Fig. 7. The discharge capacity of the pure Laves phase increases slowly as a function of the cycle number and needs 26 cycles to reach its maximum. With the addition of La or Ce, both alloys require only 10 cycles for activation and the full capacity

Table 5
Characterization of multicomponent alloys

Alloy	Phases	Cell parameter (Å)	Composition (at.%)						
			Zr	Ni	Mn	V	Cr	La	Ce
$ZrNi_{1.2}Mn_{0.6}V_{0.2}Cr_{0.1}$	C15	a=7.072	0.96	1.12	0.58	0.21	0.1	–	–
$ZrNi_{1.2}Mn_{0.6}V_{0.2}Cr_{0.1}La_{0.05}$	C15	a=7.074	0.97	1.13	0.58	0.21	0.1		–
	LaNi			49.4				50.1	–
$ZrNi_{1.2}Mn_{0.6}V_{0.2}Cr_{0.1}Ce_{0.05}$	C15	a=7.074	0.96	1.13	0.58	0.21	0.1	–	
	CeNi			49.5				–	49.25

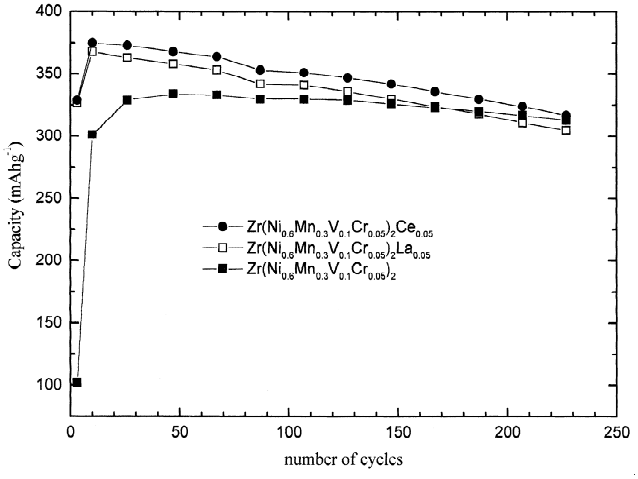

Fig. 7. Dependence of discharge electrochemical capacities on cycling.

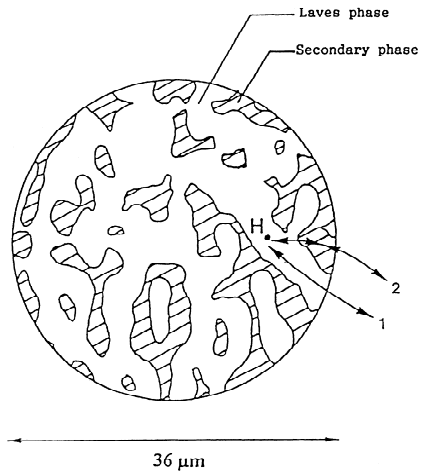

Fig. 8. Schematic microstructure of two-phase alloys and possible diffusion paths for hydrogen: (1) directly to the Laves phase (2) through the secondary phase.

increases by about 10% (from 330 to 370 mAh g^{-1}) compared to the pure Laves phase.

The morphology of grains after 24 cycles indicates clearly that the particle size of the rare earth containing alloys is smaller than that of Laves phase [8]. This implies that after adding rare earths the alloys have become much more cracked owing to the hydride formation of $RNiH_x$ accompanied by a large volume expansion. The mechanism leading to the improvement of the hydrogen absorbing properties can be described as in the previous model alloys: the dispersive LaNi and CeNi phases in the Laves phase matrix act as active sites which allow hydrogen atoms to enter through the oxide layer at the surface of the grains.

5. Conclusion

The improvement of the activation behaviour and the enhancement of the capacity due to the presence of secondary phases of different compositions has been observed for pseudobinary and multicomponent zirconium Laves phase alloys. These features can be explained by the modification of surface properties of the grains. In spite of their different compositions the two types of secondary phases have the same characteristics, which are needed to act as active sites in the surface oxide layer:

(i) The secondary phases must be homogeneously dispersed in the matrix with a particle size sufficiently small (<10 μm) in comparison to the primary phase to insure their presence at the surface of the grains during cycling after decrepitation. The Laves phase benefits the presence inside the grain of a new surface between the secondary phase and the electrolyte, which means that its charge and discharge can proceed through this surface by hydrogen diffusion through the secondary phase (Fig. 8).

(ii) The ability of these phases to form stable hydrides (which is the case for both Zr_7Ni_{10} and RNi) facilitates hydrogen diffusion. Moreover the presence of this hydride increases the decrepitation and creates fresh surfaces for hydriding more grains.

A similar phenomenon to that described here has been observed by Gutjahr et al. [13] in the discharge of alloys of the Ti–Ni system. The two phases TiNi and Ti_2Ni have low capacities due to small hydrogen absorption capacity for the former and the formation of a passivation layer for the latter. The coexistence of the two phases in a metallurgical composite favours to the charge and discharge of Ti_2Ni through the TiNi phase.

References

[1] J.-M. Joubert, M. Latroche, A. Percheron-Guégan, I. Ansara, J. Phase Equilib. 16(6) (1995) 485.
[2] J.-M. Joubert, M. Latroche, A. Percheron-Guégan, J. Bouet, J. Alloys Comp. 240 (1996) 219.
[3] S.R. Kim, J.Y. Lee, J. Alloys Comp. 185 (1992) L1.
[4] F.J. Liu, G. Sandrock, S. Suda, J. Alloys Comp. 231 (1995) 392.
[5] F.J. Liu, S. Suda, J. Alloys Comp. 231 (1995) 1066.
[6] Dalin Sun, J.-M. Joubert, M. Latroche, A. Percheron-Guégan, J. Alloys Comp. 239 (1996) 193.
[7] T. Gamo, Y. Tsuji and Moriwaki, Proc. Symp. Hydrogen and Metal Hydride Batteries, P.D. Bennet and T. Sakai (eds.), The Electrochemical Society, New York, (1994) 163.
[8] Dalin Sun, M. Latroche and A. Percheron-Guégan, J. Alloys Comp., in press.
[9] A. Züttel, F. Meli, L. Schlapbach, J. Alloys Comp. 209 (1994) 99.
[10] J.-M. Joubert, M. Latroche, A. Percheron-Guégan, J. Alloys Comp. 231 (1995) 494.
[11] A. Züttel, F. Meli, D. Chartouni, L. Schlapbach, F. Lichtenberg, B. Friedrich, J. Alloys Comp. 239 (1996) 175.
[12] K.H.J. Buschow, P.C.P. Bouten, A.R. Miedema, Rep. Prog. Phys. 4 (1982) 937.
[13] M.A. Gutjahr, H. Buchner, K.D. Beccu and H. Saufferer, Power Sources Symp., Brighton, (1972) 79.